Data-driven turbulence modeling for wind turbine wakes under neutral conditions

Steiner, Julia; Dwight, Richard; Viré, Axelle

DOI
10.1088/1742-6596/1618/6/062051

Publication date
2020

Document Version
Final published version

Published in
Journal of Physics: Conference Series

Data-driven turbulence modeling for wind turbine wakes under neutral conditions

Data-driven turbulence modeling for wind turbine wakes under neutral conditions

Julia Steiner, Richard Dwight, Axelle Viré
Wind energy research group, Aerospace faculty, Kluyverweg 1, 2629 HS Delft, Netherlands
E-mail: j.steiner@tudelft.nl

Abstract. Currently, the state of the art in wind farm flow physics modeling are Large Eddy Simulations (LES) which resolve a large part of the spectra of the turbulent fluctuations. But this type of model requires extensive computational resources. One wind speed and direction simulation of the Lillgrund wind farm can take between $160k$ and $3000k$ processor hours depending on how the turbines are modeled [1, 2]. The next-fidelity model types are Reynolds-Averaged Navier-Stokes (RANS) models which resolve only the mean quantities and model the effect of turbulence fluctuations. These models require about two orders of magnitude less computational time, but generally do not produce accurate predictions of the mean flow field. Proposed modifications made to these models so far do not generalize well and there is room for improvement. Hence, we present the first steps towards using a data-driven approach to aid in deriving new RANS models that generalize well to different turbine types, varying atmospheric stability, and farm layouts. To do so, time-averaged LES data is used to derive corrections to existing RANS models. The approach uses a deterministic symbolic regression method to infer algebraic correction terms to the RANS turbulence transport equations. Optimal correction terms to the RANS equations are derived using a frozen approach where time-averaged flow fields from LES are injected into the RANS equations. The potential of the approach is demonstrated under neutral conditions for multi-turbine constellations at wind-tunnel scale. The results show promise, but more work is necessary to realize the full potential of the approach.

1. Introduction

Offshore wind farms have the potential to become the sustainable future power plants of North-Western Europe. The Dutch government projects a growth towards 11.5 GW of installed offshore capacity in 2030, entailing that a large part of the North Sea will be filled with wind farms.

Accurate wind turbine wake models are important, because they can help optimize energy yield and turbine loading during the design and operational phase of a wind farm. There exist a multitude of models that attempt to model wake effects varying in physical fidelity, accuracy and computational cost, ranging from simple engineering models to complex computational fluid dynamics codes [3]. Generally, engineering models are not accurate enough especially if wake interaction is present. Current, state of the art are Large Eddy Simulations (LES) which is a high fidelity Computational Fluid Dynamics (CFD) method where most of the turbulent scales are resolved with the remaining ones modeled. Reynolds-Averaged Navier-Stokes (RANS) models are much faster because they model all scales resulting in coarser meshes and direct equations for the mean quantities without a need for time-averaging of the simulation. Of course, sometimes also transient quantities are of interest and the atmospheric boundary layer is inherently transient, but RANS models can still provide useful information for time-averaged

quantities over short intervals. For both RANS and LES the range of scales present, ranging from the boundary layer on the turbine blades to the height of the atmospheric boundary layer, is too large to be fully resolved. Generally, actuator models are used to model the presence of the wind turbines [4].

In this paper, we aim to further extend the capabilities of RANS turbulence models for wind turbines under (quasi) steady conditions. Currently, the most commonly used RANS model, namely the k-ϵ model, has crippling structural shortcomings: It overpredicts the eddy viscosity in the near wake which leads to an overprediction of the wake recovery and it fails to model the anisotropy of the turbulence quantities [4]. There are two main reasons why the model does not perform well in the near wake: because (i) the eddy viscosity assumption is not valid in the near wake region and (ii) the effect of the turbine on the turbulence mean quantities is not considered in the transport equations of the turbulence model [5]. Several modifications to the baseline k-ϵ model have been proposed in the literature. Most approaches aim at extending the baseline Linear Eddy Viscosity Model (LEVM) by either adding additional terms to the transport equations or by directly adding an eddy viscosity limiter in the momentum equation. El Kasmi and Masson used [6] a modified version of the k-ϵ model which introduces new source terms in the transport equations of the turbulence model. They argue that the source term in the dissipation rate equation suppresses the overproduction of turbulent kinetic energy in the near wake where strong shear gradients are present. Prospathopoulos et al. [7] apply an eddy viscosity limiter (Durbin limiter) based on a realizability constraint. Réthoré [5] used two different eddy viscosity limiters based on a realizability constraint, and the adverse pressure gradient in the near wake region. Van der Laan et al. [8] developed a model named the k-ϵ-f_P model with a limiter that reduces the eddy viscosity in regions with high-velocity gradients. The limiter is a simplified version of a cubic nonlinear EVM and is applied directly in the relation for the eddy viscosity. In a follow-up publication, van der Laan et al. [9] compare this eddy viscosity limiter to the one from Shih and Durbin, all for the k-ϵ model. They recommend the use of either the f_P or the Shih limiter since the Durbin limiter is very sensitive to ambient turbulence levels.

Alternatively, Gomez-Elvira et al. [16] and van der Laan et al. [22] also used non-linear eddy viscosity models (NLEVM) which yielded improved predictions of velocity and Reynolds stresses. However, the models they used were not robust and showed convergence issues for high turbulence intensity and fine meshes. Cabezon et al. [11] also used a Reynolds Stress Model (RSM) which again improved predictions but the model was not numerically robust. Additionally, RSM models are also more expensive, because seven transport equations have to be solved.

While all of these models offer some improvements over the standard k-ϵ model, the improvements are test-case dependent, some of them require tuning parameters, are not numerically robust and at this point, the influence of atmospheric stratification is not considered. Further, while most of these models aim at improving the shortcomings of the eddy viscosity assumption, they do not directly consider the effect of actuator forcing on the turbulence equations.

In this publication we take a different approach, namely, this work contains the first step towards a data-driven general and robust RANS model for wind farm applications. As such an improved model, trained on time-averaged LES data, is presented for several multi-turbine constellations at wind tunnel scale under neutral conditions. From an application point of view, this is a limited dataset. However, given that data-driven turbulence models are a relatively new development in the fluid dynamics community and their merit has only been shown for fundamental cases, this publication aims at applying this methodology to more industrially relevant flows [15]. The only examples of data-driven turbulence modeling for wind farms that are known to the authors are Adcock et al. [10] and King et al. [17]. Both papers employ similar

techniques but do not present results that go beyond a two-dimensional setup.

2. Methodology

This section will describe the entire data-driven turbulence modeling approach: data generation with LES, correction to the RANS baseline turbulence model and finally, the data-driven approach to train a closure model. This section is kept brief, but references to more detailed descriptions are given.

2.1. Setup case database

The first step in the proposed methodology is to set up a database of cases that can be used to both train and validate the correction terms. For this publication, the database consisted of three different cases. The same surface roughness and hub height velocity were used for all the cases, but the turbine constellation was changed, as visualized in Figure 2. The turbine and inflow properties correspond to the wind tunnel experiment from Chamorro and Porté-Agel [12], the most important parameters are listed in Figure 2.

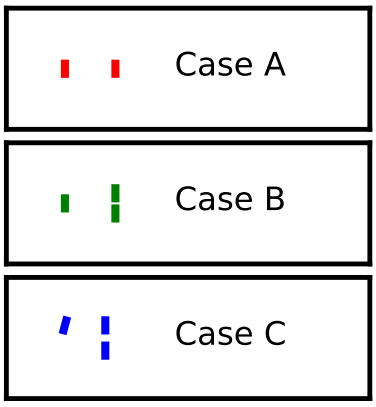

Figure 1. Case constellation, turbine diameter is to scale.

Turbine	
Diameter	$D = 0.15$m
Hub height	$h_{hub} = 0.125$m
Rotation speed	$\Omega = 1190$rpm
Inflow boundary	**layer**
Velocity	$U\,(h_{hub}) = 2.2$m/s
Turbulence intensity	$\sigma_U\,(h_{hub}) = 0.09\%$
Mesh	
Domain size	$5.4 \times 1.8 \times 0.46\text{m}^3$
Resolution	$288 \times 48 \times 64$

Figure 2. Turbine and inflow parameters

For the CFD model, OpenFOAM-6.0 is used in conjunction with the SOWFA-6 toolbox [13]. For the RANS solver, a modified k-ϵ model is used and for the LES solver, the Wale model is used to model the unresolved scales [14, 19]. A validation of both turbulence models is carried out on the benchmark case from Chamorro and Porte-Agél. Additionally, Xie and Archer's results are used to determine an appropriate mesh resolution for the LES simulations [21]. SOWFA's actuator disk model with the same parameters is used in both the RANS and LES simulations. For simplicity and to avoid interpolation errors, the same mesh resolution was used for both RANS and LES, even though the RANS simulations would be able to run with a lower resolution than the LES ones.

Figure 3 shows the validation of the models on the benchmark case in terms of velocity and turbulence intensity. As expected RANS tends to overpredict turbulence intensity and wake recovery as compared to LES. Nevertheless, neither one of the models perfectly matches the experiment, possibly also due to the low Reynolds number of the Wind Tunnel setup since the wall functions and the RANS turbulence model are derived for larger Reynolds numbers. Hence, the authors would like to stress that the aim of this publication is not to perfectly reproduce the experiments, but to showcase the potential of a methodology that can help to systematically improve RANS based predictions, also at full scale.

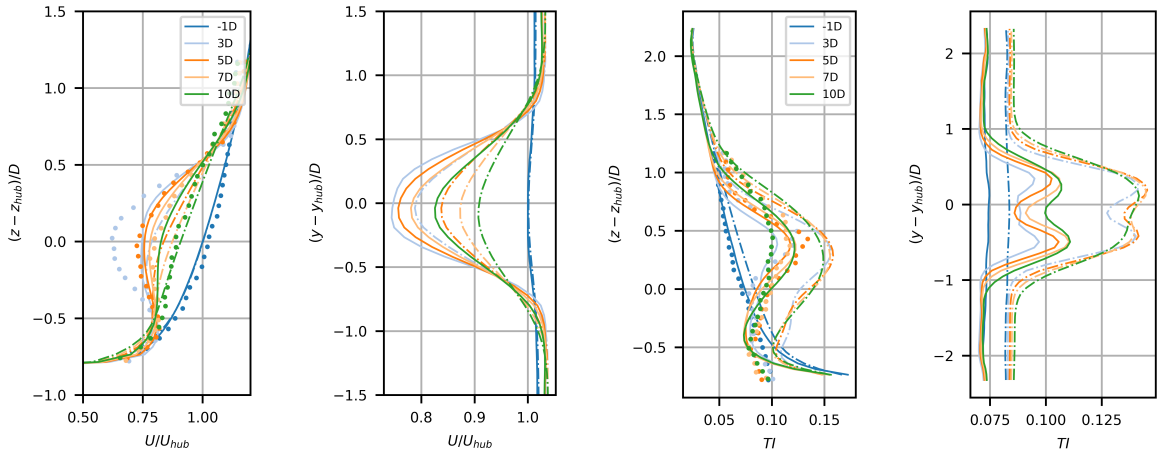

Figure 3. Validation of case setup and turbulence models through vertical and horizontal slices of the flow field up and downstream of the rotor plane in terms of velocity and turbulence intensity, solid line corresponds to LES, dash dotted line corresponds to RANS, and dots belong to experimental results

2.2. Derivation of optimal correction terms

The first step in improving RANS predictions is to find an optimal way to correct the RANS equations such that they match the time-averaged LES results in terms of mean velocity and turbulence intensity. The approach presented here was developed by Schmelzer et al. [20]. The turbulence equations of the RANS model are solved with the frozen time-averaged LES fields for velocity $\overline{u}^{LES}$, turbulent kinetic energy $\overline{k}^{LES}$ and Reynolds stresses $\overline{\tau}_{ij}^{LES}$. Where both the resolved and modeled turbulent quantities are used. Two correction terms are added to the transport equations for k and ϵ: A correction of the anisotropy tensor b_{ij}^{Δ} and a correction for the turbulent kinetic energy production $\mathcal{P}_k^{\Delta}$. These correction terms are embedded in the two transport equations as follows

$$\frac{D\hat{k}}{Dt} = \hat{\mathcal{P}}_k + \mathcal{P}_k^{\Delta} - \epsilon + \frac{\partial}{\partial x_j}\left[\left(\nu + \sigma_k \nu_t\right)\hat{k}\right], \tag{1}$$

$$\frac{D\epsilon}{Dt} = \left[C_{\epsilon 1}\left(\hat{\mathcal{P}}_k + \mathcal{P}_k^{\Delta}\right) - C_{\epsilon 2}\epsilon\right] \cdot \frac{\epsilon}{\hat{k}} + \frac{\partial}{\partial x_j}\left[\left(\nu + \sigma_\epsilon \nu_t\right)\epsilon\right] \tag{2}$$

with the production term

$$\hat{\mathcal{P}}_k = 2\hat{k}\hat{b}_{ij}\frac{\partial \hat{u}_i}{\partial x_j} \text{ by definition of } \hat{b}_{ij} = \frac{1}{2\hat{k}}\left(\hat{b}_{ij} + \frac{1}{3}\delta_{ij}\right) = -\frac{\nu_t}{\hat{k}}\hat{S}_{ij} + b_{ij}^{\Delta}. \tag{3}$$

where frozen terms obtained from LES are marked with $\hat{x} = \overline{x}^{LES}$. The two correction terms and the turbulent dissipation are obtained through iterative solving of the two transport equations.

2.3. Learning of correction terms

Once the optimal correction terms $\mathcal{P}_k^{\Delta}$ and b_{ij}^{Δ} are known, a generalized expression for the correction terms is inferred using a deterministic symbolic regression method similar to the one presented in Schmelzer et al. [20]. For this a generalized nonlinear eddy viscosity formulation

as proposed by Pope [18] is used. The normalized anisotropic part of the Reynolds stress tensor can then be modelled as a linear combination of ten basis tensor $T_{ij}^{(n)}$ and functional expressions α_n dependent on five invariants I_n:

$$b_{ij}^{\Delta}\left(S_{ij},\Omega_{ij}\right)=\sum_{n=1}^{10}T_{ij}^{(n)}\alpha_n\left(I_1,\ldots,I_5\right)\leftrightarrow b_{ij}^{\Delta}\left(S_{ij}^n,\Omega_{ij}^n\right)=C\Theta. \tag{4}$$

where both the tensors as well as the invariants are constructed based on the strain rate $S_{ij}=\frac{1}{2}\left(\partial_j U_i+\partial_i U_j\right)$ and the rotation rate tensor $\Omega_{ij}=\frac{1}{2}\left(\partial_j U_i-\partial_i U_j\right)$.The entire equation can be rewritten into a linear system of equations with coefficients Θ and system matrix C.

A similar approach is taken for the production correction term $\mathcal{P}_k^{\Delta}$

$$\mathcal{P}_k^{\Delta}\left(S_{ij},\Omega_{ij}\right)=2k\sum_{n=1}^{N=10}T_{ij}^{(n)}\alpha_n^R\left(I_1,\ldots,I_5\right)\frac{\partial u_i}{\partial x_j}\leftrightarrow\mathcal{P}_k^{\Delta}\left(S_{ij}^n,\Omega_{ij}^n\right)=C^R\Theta^R. \tag{5}$$

The task of the machine learning algorithm is then to find a suitable formulation for the functions α_n, based on a linear combination of a library of candidate functions. In principle, then a least-squares approach can be used to find the optimal coefficients Θ. However, Schmelzer et al. [20] argue that this yields unnecessarily complex models that may be overfitting the data. Further, due to multi-collinearity in the input data, large differences in the magnitude of the coefficients may result. Yet, such models are unsuitable for implementation in CFD models as they may produce numerically stiff systems. Hence, a different sparsity promoting approach is used here. The outline of the procedure is:

(i) **Model discovery** using Lasso regression to identify important terms. The end result is an array of models with different complexity obtained by varying the regularization parameters λ and ρ. The parameters have to be varied because their optimal values are not known a priori.

$$\Theta=\min_{\hat{\Theta}}\left[\left\|C\hat{\Theta}-b_{ij}^{\Delta}\right\|_2^2+\lambda\rho\left\|\hat{\Theta}\right\|_1+0.5\lambda(1-\rho)\left\|\hat{\Theta}\right\|_2^2\right] \tag{6}$$

(ii) **Remove unnecessary entries** from library $C\rightarrow\tilde{C}$ and $\Theta\rightarrow\tilde{\Theta}$.

(iii) **Model calibration** using Ridge regression to identify magnitude of model coefficients for all the previously derived array of corrections. Again a regularization parameter λ_R is used to ensure that the magnitude difference between the differenct coefficients is not too large.

$$\tilde{\Theta}=\min_{\hat{\Theta}}\left[\left\|\tilde{C}\hat{\Theta}-b_{ij}^{\Delta}\right\|_2^2+\lambda_r\left\|\hat{\Theta}\right\|_2^2\right] \tag{7}$$

For a more detailed description of the approach see Schmelzer et al. [20].

Finally, since the models give explicit expressions for the correction terms, they can be directly integrated into the RANS model. Practically speaking, usually, some under-relaxation is necessary, especially for the anisotropy correction.

3. Results and discussion

This section will show the application of the proposed methodology to the previously described dataset. Resulting flow fields with the optimal and the learned correction terms are shown and discrepancies are discussed in detail.

3.1. Flow field with optimal correction terms

The optimal correction terms are derived for the three cases in the dataset. Subsequently, the optimal corrections are integrated into to the RANS turbulence models for all the three test cases. The results obtained from this are referred to as frozen or optimally corrected RANS. Figures 5 and 6 show the wake development as predicted by the LES, the baseline RANS and the frozen RANS simulations. The latter ones represent the best-case scenario that can be obtained when using this methodology. In the next subsection, the generalized models for the correction terms will introduce additional errors. The results in the figure show that indeed the optimal correction terms lead to an almost perfect match between LES mean and frozen RANS velocity and turbulent kinetic energy fields.

3.2. Learning of correction terms

The results presented in the following are based on a merged dataset for the three constellations presented in Figure 2. The dataset is randomly split into a training and test dataset with 80 % of the data being used for training and the remainder for testing.

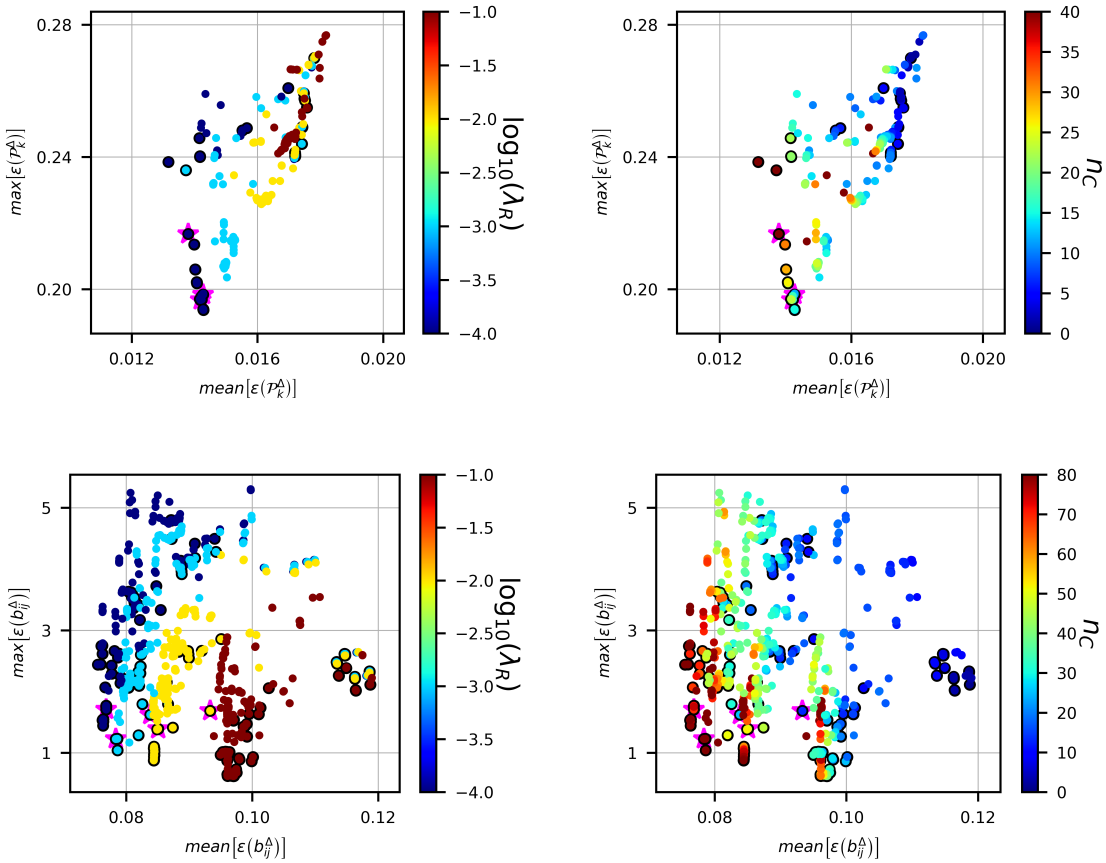

Figure 4. Scatter plot of all the models obtained for both correction terms. Members of the three-dimensional pareto front with respect to mean and max error, as well as model complexity are highlighted in black. The coloring of the elements is according to the magnitude of the Ridge λ_R penalization parameter and the model complexity n_C .

Following the methdology outlined previously, the feature set used to construct a library

of basis functions consists of the first and the second invariant of Pope's integrity basis $I_1 = \text{trace}\left(S^2\right)$, $I_2 = \text{trace}\left(\Omega^2\right)$, and additonally the wall distance based Reynolds number $\text{Re}_z = \min\left(5.0, \frac{\sqrt{k}z}{50\nu}\right)$. The latter one is important for the model to be able to distinguish between the boundary layer and the shear layer in the wake. Additionally, only the first four tensors of the integrity basis are used where $T^{(1)} = S$, $T^{(2)} = S\Omega - \Omega S$, $T^{(3)} = \text{dev}\left(S^2\right)$, $T^{(4)} = \text{dev}\left(\Omega^2\right)$ where dev is the deviatoric part of the tensor. The features are then combined with each other and each other squares to form basis expressions for the scalar functions α_n and α_n^R.

The three-step regularization methodology is applied to determine, first which coefficients are important, and second what the magnitude of these coefficients should be. Figure 4 shows the results of this process for both the anisotropy and the turbulence kinetic energy correction term. The left side of the figure illustrates the trade-off between the robustness and the model accuracy by showing the influence of the Ridge regularization parameter λ_R on the mean and maximum error of the model on the test data set. The right side of the figure visualizes the trade-off between the model complexity and the model accuracy by highlighting the number of terms of the model. But the results are not straight-forward, complex models do not necessarily give better predictions and while higher regularization does correlate with a higher mean error it tends to also reduce the maximum error. Because the process generates a lot of models and it was difficult to pick which models to be used going forward, the three-dimensional Pareto front in terms of mean error, maximum error, and model complexity is also shown in the figure. The members of the Pareto front which are highlighted with a star were investigated further in the following paragraphs. Three different models for the turbulent kinetic energy production and five for the anisotropy correction term were picked. The chosen models were picked to have varying degrees of complexity while providing a sufficient amount of accuracy. For both correction terms also one model each was picked that was obtained with a direct least square approach to estimate the maximum accuracy that can be reached with the given library.

3.3. Flow field with learned correction terms

Once the models for the correction terms are derived, an intermediate step between implementing the corrections in the turbulence model is taken: namely, the correction terms are calculated once based on the LES mean fields for the cases and then injected into the RANS simulations. Figures 5 and 6 show the resulting flow fields for the baseline model, the frozen case and the models with a constant correction. All possible combinations between the eight models chosen in the previous subsection were tested and the spread between the models is shown in the figure. As can be seen, all corrections yield significant improvement over the baseline model and the difference between the different corrections terms is much smaller than the overall improvement as compared to the baseline case.

Since the results with the constant correction terms indicate that the simplest proposed models already yield a significant improvement as compared to the baseline case, the two simplest correction terms are implemented in the RANS turbulence model such that they are directly coupled to the RANS flow field. The chosen terms are written out below

$$\begin{aligned}\mathcal{P}_k^{\Delta} = 2k\frac{\partial u_i}{\partial x_j}(&\mathbf{T}_{ij}^{(1)} \cdot [1.30 \cdot 10^{-2} + 5.15 \cdot 10^{-5} I_1 - 7.35 \cdot 10^{-6} I_2 + 1.34 \cdot 10^{-2} m_2 + 2.27 \cdot 10^{-9} I_1 I_2 m_2 \\ &+5.72 \cdot 10^{-10} I_1 I_2 m_2^2 + 1.05 \cdot 10^{-7} I_1 m_2^3 + 1.05 \cdot 10^{-9} I_1^2 m_2 + 8.97 \cdot 10^{-11} I_1^2 m_2^2 \\ &+1.11 \cdot 10^{-6} I_2 m_2^2 - 1.70 \cdot 10^{-7} I_2 m_2^3 + 1.20 \cdot 10^{-9} I_2^2 m_2 + 1.34 \cdot 10^{-10} I_2^2 m_2^2 \\ &-2.53 \cdot 10^{-3} m_2^2] \\ &+\mathbf{T}_{ij}^{(3)} \cdot [1.09 \cdot 10^{-3} + 5.40 \cdot 10^{-3} m_2 - 1.03 \cdot 10^{-3} m_2^2] \\ &+\mathbf{T}_{ij}^{(4)} \cdot 4.30 \cdot 10^{-3})\end{aligned} \tag{8}$$

and

$$\begin{aligned}b_{ij}^{\Delta} = &\mathbf{T}_{ij}^{(1)} \cdot [9.21 \cdot 10^{-6} I_2 + 4.14 \cdot 10^{-5} I_1] \\ &+\mathbf{T}_{ij}^{(2)} \cdot [-1.27 \cdot 10^{-9} I_1 I_2 - 1.09 \cdot 10^{-5} I_1 m_3^3 - 2.50 \cdot 10^{-6} I_1 m_3^4 - 3.69 \cdot 10^{-10} I_1^2 \\ &\quad +6.78 \cdot 10^{-6} I_2 + 2.04 \cdot 10^{-9} I_2^2 - 1.81 \cdot 10^{-3} m_3 + 2.79 \cdot 10^{-3} m_3^2 + 3.72 \cdot 10^{-3}] \\ &+\mathbf{T}_{ij}^{(3)} \cdot 1.32 \cdot 10^{-3} \\ &-\mathbf{T}_{ij}^{(4)} \cdot 6.54 \cdot 10^{-4}\end{aligned} \tag{9}$$

where $m_2 = \min(Re_z, 5.0)$ and $m_3 = \mathrm{Re}_z$ if $\mathrm{Re}_z < 5.0$ and otherwise $m_3 = 0$.

The results obtained with the coupled correction terms are shown in Figures 5 and 6 as well. Unfortunately, the corrected results now lie closer to the baseline ones than the frozen ones. There are several reasons for this. The most obvious one being the inaccuracy in the prediction of the correction terms. Even small errors in the prediction can self-amplify themselves due to the coupling with the velocity field and the turbine forcing. This holds in particular for the prediction for the normal components of the anisotropy correction. In fact, the predictions showed some oscillations near the turbines for the normal components and hence only 70 % of the anisotropy correction term was imposed, otherwise, the simulations were not stable. That is why the figure does not only show the results for the model with both learned correction terms, but also the ones with no correction for the anisotropy and the ones with the optimal anisotropy correction. As visible from the figure, the model with no anisotropy correction is closer to the baseline case than the frozen one. The one with the optimal anisotropy correction generally is close to the frozen one. This shows that the turbulent production correction $\mathcal{P}_k^{\Delta}$ is working well, but more work is needed for the prediction of the anisotropy correction b_{ij}^{Δ}.

Another prominent source for the mediocre results is that the mean of the correction terms is not zero in the freestream. Hence, even though the same inflow profiles are used as for LES, in an empty domain the velocity profile will change in the streamwise direction. However, the regularization used to make the corrections more robust will drive the correction terms to zero if increased. In future work, this needs to be improved by for example having a preprocessing step which ensures that the freestream profiles match through the introduction of an additional uniform correction term.

Lastly, the learned correction terms do not match the optimal ones well close to the rotor. Possibly, also an improved input feature set that includes the turbine forces, as well as, pressure terms will improve the predictions.

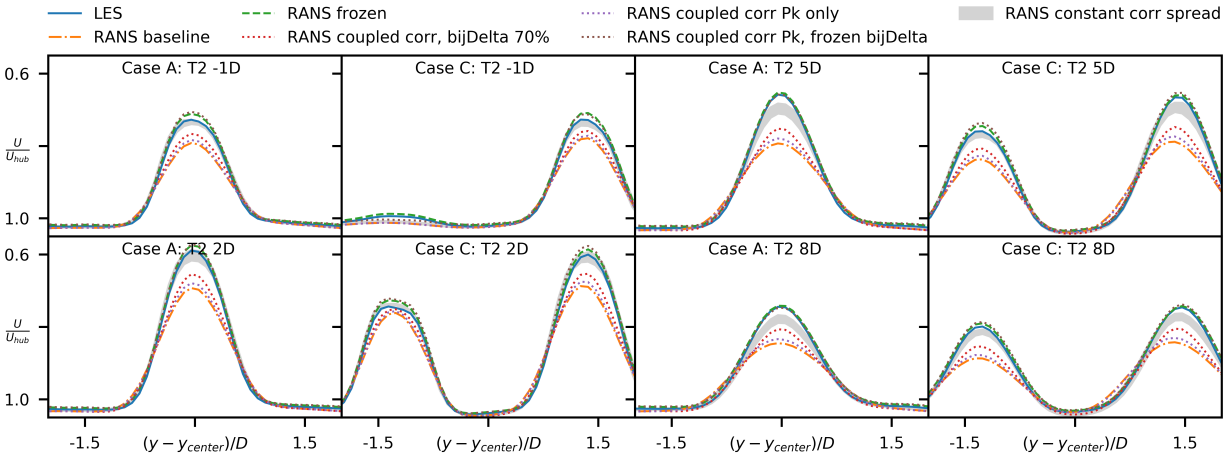

Figure 5. Comparison between LES, RANS baseline, frozen RANS and corrected RANS models via horizontal slices of the velocity field up and downstream of the rotor plane for the second turbine of case A and the second and third turbines of case C

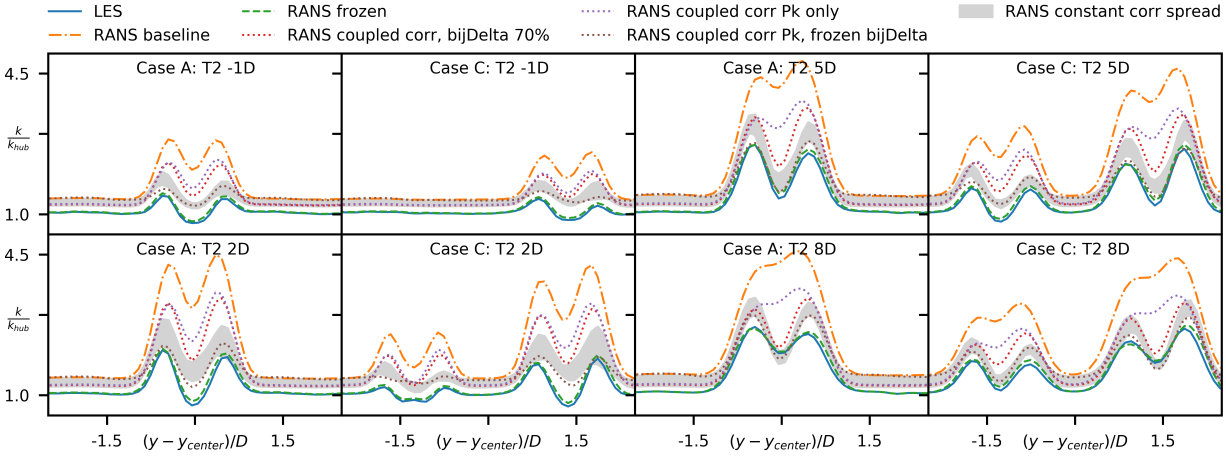

Figure 6. Comparison between LES, RANS baseline, frozen RANS and corrected RANS models via horizontal slices of the turbulent kinetic energy field up and downstream of the rotor plane for the second turbine of case A and the second and third turbines of case C

4. Conclusions

On a limited data set, the proposed frozen k-corrective-frozen-RANS showed potential for improving the predictions of the mean velocity and turbulent kinetic energy predictions. Based on time-averaged LES data optimal correction terms to the turbulence transport equation of the RANS model were determined. This part of the proposed methodology is working very well, however, learning these terms using a sparse regression approach still needs more work. In particular, the accuracy of the learned corrections for the anisotropy tensors needs to be improved through several measures. First by finding a better way to incorporate non-zero mean values of the optimal correction terms especially when they appear in the freestream. And, second by defining a larger input feature set that also makes use of the turbine forcing and the pressure gradient field such that the algorithm can distinguish between the near and the farfield of the wake. Nevertheless, given that data-driven turbulence models are a relatively new

development in the fluid dynamics community and so far they have only been applied to very fundamental cases, the obtained results are already a step in the right direction. Of course, to apply the methodology to more realistic conditions including atmospheric stratification and real scale turbines, a lot of work is still necessary.

References

[1] Breton S P, Sumner J, Sørensen J N , Hnsen K S, Sarmast S and Ivanell S 2017 A survey of modelling methods for high-fidelity wind farm simulations using large eddy simulation *Phil.Transactions of the Royal Society A: Math., Phys. and Eng. Sc.* **375** 20160097
[2] Ghaisas N S, Archer C L, Xie S, Wu S and Maguire E 2017 *Wind Energy.* **20** 1227–1240
[3] Stevens R and Meneveau C 2017 *Annual Review of Fluid Mechanics.* **49** 311–339
[4] Sanderse B, Pijl S P and Koren B 2011 *Wind Energy.* **14** 799–819
[5] Rethore P-E, Sørensen N N, Bechmann A and Zahle F 2009 *EWEC Marseille* Study of the atmospheric wake turbulence of a CFD actuator disc model
[6] El Kasmi A and Masson C 2008 *Journal of Wind Engineering and Industrial Aerodynamics.* **96** 103–122
[7] Prospathopoulos J M, Politis E S, Rados K G and Chaviaropoulos P K 2011 *Wind Energy.* **14** 285–300
[8] van der Laan P M, Sørensen N N, Rethore P-E, Mann J, Kelly M C, Troldborg N, Schepers G J and Machefaux E 2015 *Wind Energy.* **18** 889–907
[9] van der Laan M P and Andersen S J 2018 *J. Phys.: Conf. Series* **1037** 072001
[10] Adcock C and King R N 2018 *Annual American Control Conference* p 695–700
[11] Cabezon D, Migoya E and Crespo A 2011 *Wind Energy.* **14** 909–921
[12] Chamorro L P and Porté-Agel F 2010 *Boundary-Layer Meteorology.* **136** 515–533
[13] Churchfield M and Sang Lee *NWTC Information Portal (SOWFA).* https://nwtc.nrel.gov/SOWFA. (Accessed 27.02.2020)
[14] Nicoud F and Ducros F 1999 *Flow, Turbulence and Combustion.* **62** 183–200
[15] Duraisamy K, Iaccarnino G and Xiao H 2019 *Annual Review of Fluid Mechanics.* **51** 357–377
[16] Gomez-Elvira R, Crespo A Migoya E Manuel F and Hernández 2005 *Journal of Wind Engineering and Industrial Aerodynamics.* **93** 797–814
[17] King R N, Adock C, Annoni J and Dykes K 2018 *J. Phys.: Conf. Series* **1037** 072004
[18] Pope S B 1975 *Journal of Fluid Mechanics.* **72** 331–340
[19] Sanz R J, Churchfield M and Kosovic B 2017 A methodology for the design and testing of atmospheric boundary layer models for wind energy applications *Wind Energy Science* **2** 35–54
[20] Schmelzer M, Dwight R and Cinnella P 2020 *Flow Turbulence and Combustion.* **104** 579–603
[21] Xie S and Archer S 2015 *Wind Energy.* **18** 1815–1838
[22] van der Laan P M, Sørensen N N, Rethore P-E, Mann J, Kelly M C and Schepers G J 2013 *International Conference onaerodynamics of Offshore Wind Energy Systems and wakes* Nonlinear Eddy Viscosity Models applied to Wind Turbine Wakes p 514–525